Molecular Cell, Volume *82*

Supplemental information

Regulation of GTPase function by autophosphorylation

Christian W. Johnson, Hyuk-Soo Seo, Elizabeth M. Terrell, Moon-Hee Yang, Fenneke KleinJan, Teklab Gebregiworgis, Genevieve M.C. Gasmi-Seabrook, Ezekiel A. Geffken, Jimit Lakhani, Kijun Song, Puspalata Bashyal, Olesja Popow, Joao A. Paulo, Andrea Liu, Carla Mattos, Christopher B. Marshall, Mitsuhiko Ikura, Deborah K. Morrison, Sirano Dhe-Paganon, and Kevin M. Haigis

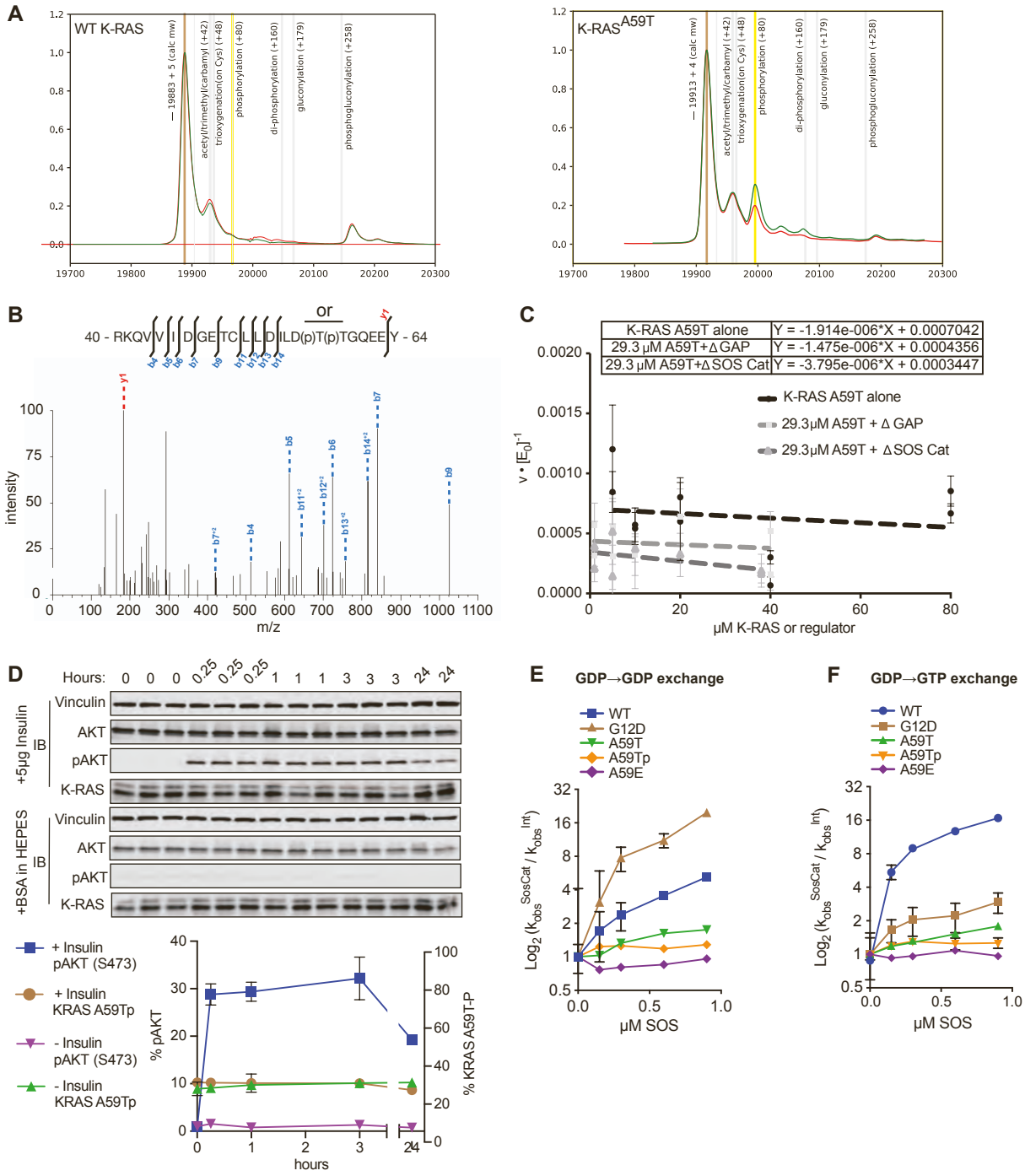

Figure S1. Kinetics of K-RAS autophosphorylation and its effect on nucleotide hydrolysis and exchange, related to Figure 1.

(A) Intact mass spectrometry of purified wildtype K-RAS4B (left) and K-RAS^{A59T} (right) protein. Proteins were incubated at 37˚C with (green line) or without (red) GTP for 6 hours before being subjected to intact mass spectrometry. Mass of unmodifed protein is shown by the brown line and the change in mass due to a single phosphorylation is shown by the yellow line.

(B) Two precursor peptides, of sequence RKQVVIDGETCLLDILDTTGQEEY, were expected for purified non-phosphorylated (precursor mass: 932.46464, charge: 3+) and phosphorylated (precursor mass: 959.12007, charge 3+) K-RAS^{A59T}. Shown is the spectrum for the phosphorylated peptide.

(C) Kinetics of Thr59 autophosphorylation in response to increasing concentrations of 6xHis-KRAS4B^{A59T} or increasing concentrations of the catalytic domains of SOS or GAP.

(D) SNU-175 cells were serum starved overnight and induced with insulin (5µg/mL). Cells were induced at the same time and then stopped at the indicated time points at the top of the blots. Replicates are labelled above the gel and quantification of bands are shown on the right. Data in the right panel were normalized to the average phosphoerylation status of AKT at 0 hours.

(E) and (F) Effects of SOS on nucleotide cycling of (E) GDP for mant-GDP and (F) GDP for mant-GTP. Data are depicted as a fold-change relative to *k* of the intrinsic exchange reaction, and data points represent average *k* assuming a first order mechanism (n = 2-4).

Error bars represent standard deviation.

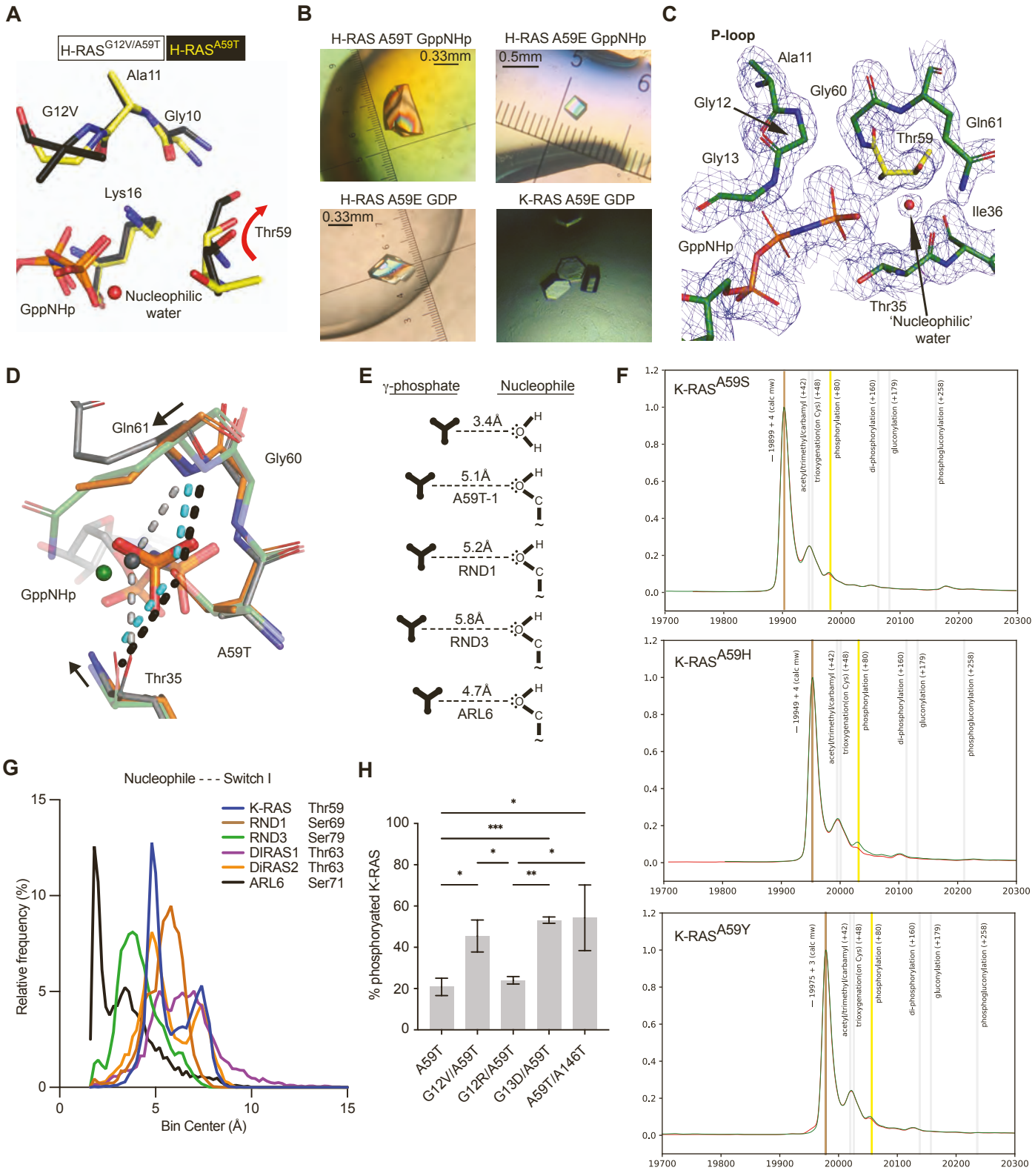

Figure S2. Crystal and dynamic data for autophosphorylation mechanism, related to Figure 2.

(A) Crystal structures of H-RAS^{A59T} (yellow) are different from a previously deposited crystal structure of H-RAS$^{G12V/A59T}$ (black, PDB code 521P) in that T59 is oriented away from the GTP in the G12V/A59T structure.

(B) Protein crystals of H-RAS and K-RAS.

(C) Active site electron density of H-RAS^{A59T} (sigma = 1.0).

(D) Comparison of H-RAS^{A59T} crystal 1 (yellow) and crystal 2 (orange) active sites. The nucleophilic water is colored according to its protein crystal. H-RAS^{A59T} crystal 2 shifts toward active site which forces the nucleophilic water molecule to be absent in this crystal.

(E) Comparison of T59 orientiation (right) and distance from the gamma-phosphate of GTP (left) in various GTPases.

(F) Intact mass spectrometry of purified K-RAS^{A59S} (top), K-RAS^{A59H} (middle), and K-RAS^{A59Y} (bottom), protein. Proteins were incubated at 37˚C with (green line) or without (red) GTP for 6 hours before being subjected to intact mass spectrometry. Mass of unmodifed protein is shown by the brown line and the change in mass due to a single phosphorylation is shown by the yellow line.

(G) Frequency distribution of nucleophile to switch I residue (labeled) distances in small GTPase MD simulations.

(H) Steady-state autophosphorylation of HA-tagged K-RAS mutants ectopically expressed in NIH3T3 cells (n=4-8). Results are from quantitative western blots with values calculated as p-K-RAS = (upper band/(upper band + lower band))*100. Signifance was calculated using Mann-Whitney U-test. * P < 0.05, **P < 0.005, and *** P < 0.0005.

Error bars represent standard deviation.

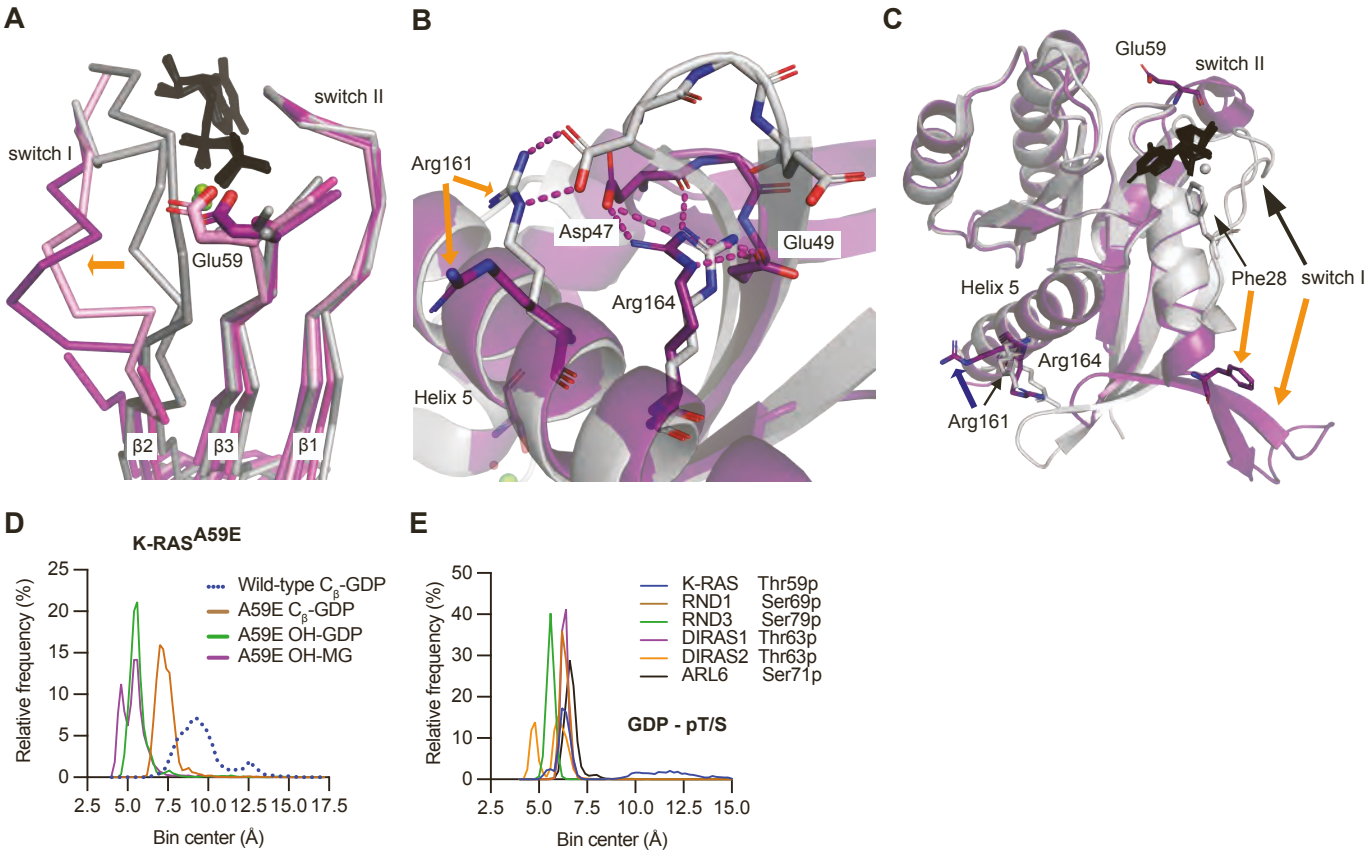

Figure S3. RAS A59E and A59Tp open the active site and increase dynamics, related to Figure 4.
(A) H-RAS^{A59E} crystal structures (magenta, purple) show that E59 breaks secondary structure interactions made between the β2 and β3.
(B) The switch I conformation of K-RAS^{A59E} GDP is stabilized by alternative salt-bridge interactions made between R164, D48, E49 and the β-turn connecting β2 and β3. Note that D47 trades its salt-bridge interaction with R161 in WT K-RAS (PDB code 4OBE, gray) for R164.
(C) The alternate switch I conformation removes the F28-K147 stacking interaction that helps stabilize binding of the guanosine base of GDP. The nucleotide is shown as black sticks on each panel.
(D-E) Frequency distributions of bond distances during MD simulations of GDP bound K-RAS mutants and other GTPases phosphorylated by *in silico* modification.

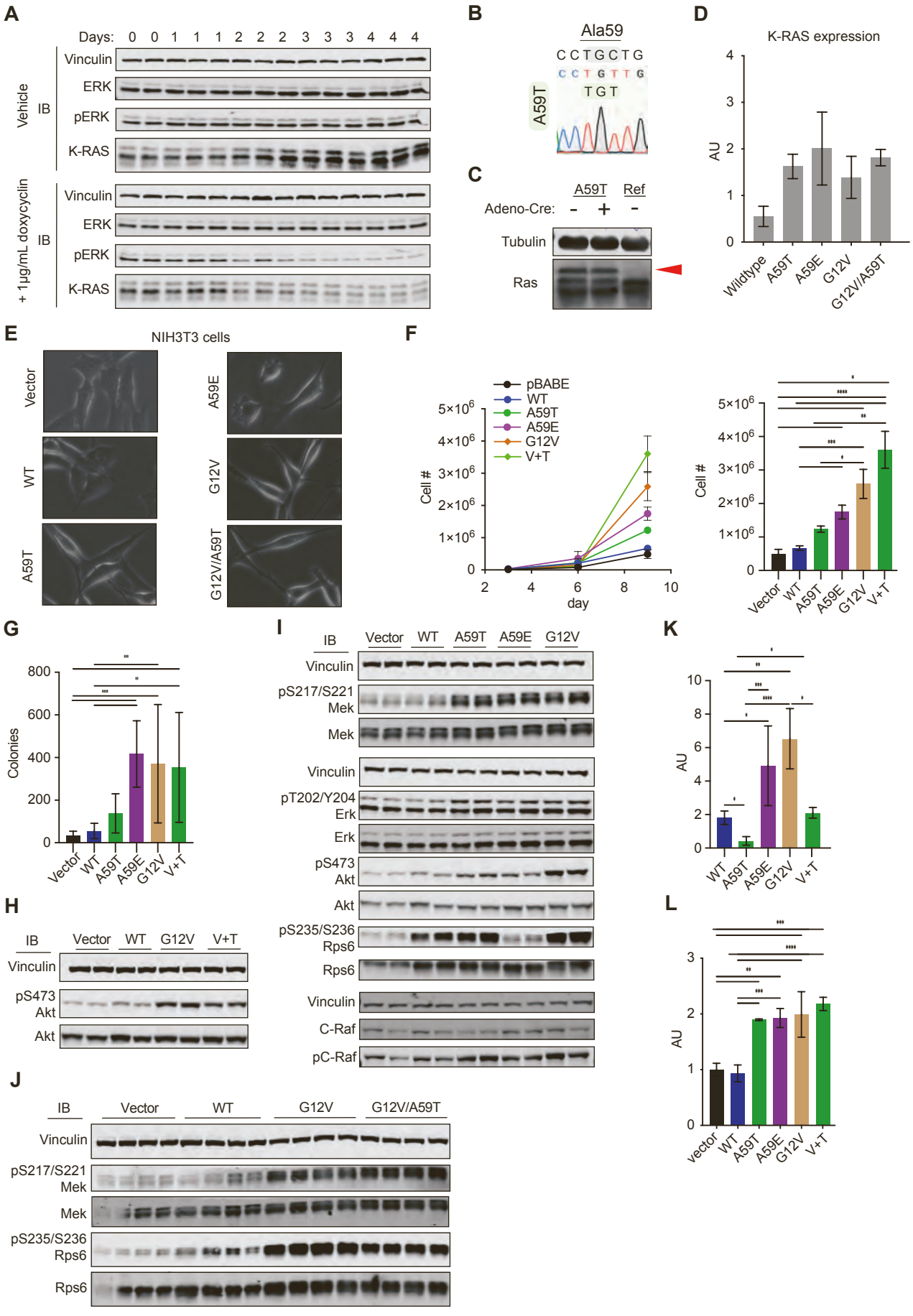
A
Days: 0 0 1 1 1 2 2 2 3 3 3 4 4 4
Vehicle
IB
Vinculin
ERK
pERK
K-RAS
+ 1µg/mL doxycyclin
IB
Vinculin
ERK
pERK
K-RAS
B
Ala59
C C T G C T G
C C T G T T G
T G T
A59T
C
A59T Ref
Adeno-Cre: - + -
Tubulin
Ras
D
K-RAS expression
AU
Wildtype
A59T
A59E
G12V
G12V/A59T
E
NIH3T3 cells
Vector
WT
A59T
A59E
G12V
G12V/A59T
F
pBABE
WT
A59T
A59E
G12V
V+T
Cell #
day
Cell #
Vector
WT
A59T
A59E
G12V
V+T
G
Colonies
Vector
WT
A59T
A59E
G12V
V+T
H
IB
Vector
WT
G12V
V+T
Vinculin
pS473 Akt
Akt
I
IB
Vector
WT
A59T
A59E
G12V
Vinculin
pS217/S221 Mek
Mek
Vinculin
pT202/Y204 Erk
Erk
pS473 Akt
Akt
pS235/S236 Rps6
Rps6
Vinculin
C-Raf
pC-Raf
K
AU
WT
A59T
A59E
G12V
V+T
L
AU
Vector
WT
A59T
A59E
G12V
V+T
J
IB
Vector
WT
G12V
G12V/A59T
Vinculin
pS217/S221 Mek
Mek
pS235/S236 Rps6
Rps6

Figure S4. Role of K-RAS^{A59T} and K-RAS^{A59E} in cell transformation, related to Figure 4.

(A) The effect of K-RAS knockdown on the phosphorylated state of K-RAS^{A59T} after induction of shRNA by 1μg/mL of doxycyclin was measured in replicates over the indicated days.

(B) Sequencing chromatogram of PCR product of exon 2 showing codon 59. DNA are taken from CRISPR modified mouse embryonic stem cells.

(C) Western blot of protein expression from mouse embryonic stem cells with K-Ras^{A59T}, with and without Adeno-Cre, confirming the homozygosity of the A59T mutation in our CRISPR modified mES cells. Right most lane is a stem cell line with wildtype K-Ras. Red arrow denotes the upper phosphorylated band also present in these cells.

(D) Quantification of western blot for HA-tagged K-RAS4B in NIH3T3 cells (n=4-12).

(E) Morphologies of NIH3T3 cells expressing different K-RAS proteins. All images were taken at the same scale.

(F) Left, Cell proliferation of NIH3T3 cells expressing different mutants of K-RAS grown in 10% FBS (n=4-5). Right, quantification and statistics of cell growth after nine days. V+T refers to G12V/A59T.

(G) Soft-agar growth of fibroblasts expressing different K-RAS proteins (n=3).

(H-J) Representative western blots of MAPK and AKT signaling pathway proteins from NIH3T3 cells expressing different mutants of K-RAS. Black bar over lanes represent replicates.

(K) Statistics of quantified C-RAF-RBD pulldowns from Figure 4. Data are scaled to K-RAS expression (D).

(L) Statistics of quantified Mek phosphorylation from Figure 4.

Error bars represent standard deviation and statistical analyses were performed with Mann-Witney tests. *, **, ***, **** represent P-values of <0.05, <0.005, and <0.0005.

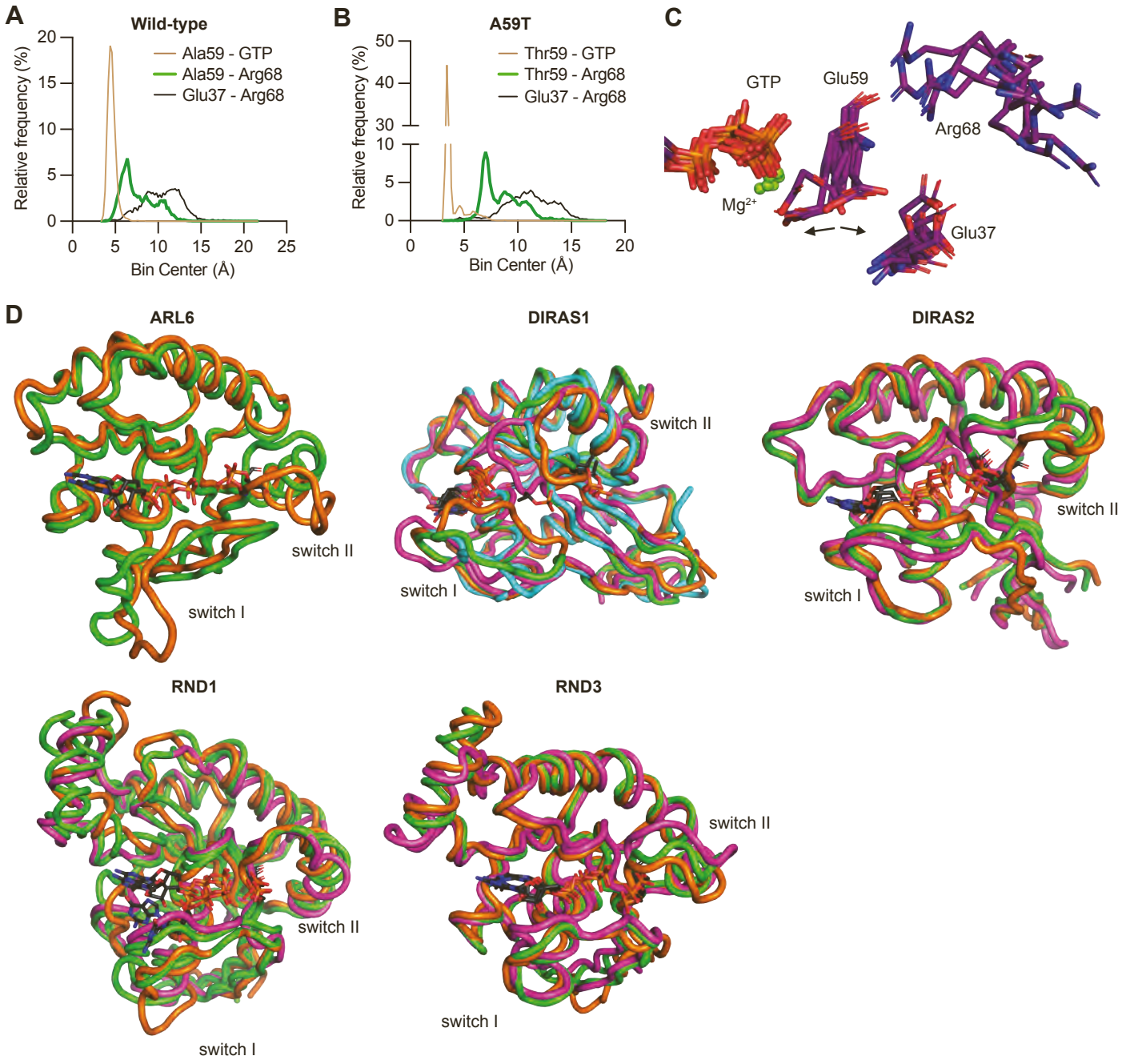

Figure S5. Dynamics of phosphorylated or phospho-mimetic residue 59, related to Figure 5.
(A) and (B), Frequency distributions of bond distances during MD simulations of GDP bound K-RAS mutants and auto-phosphorylating GTPases phosphorylated by *in silico* modification.
(C) Simulation cluster analysis of K-RAS^{A59E} bound to GTP with a 0.2nm cutoff distance between frames.
(D) Cluster analysis of simulations of aGTPase structures starting in the GTP bound state or exchanged to GTP, and with residue 59 modified with phosphorylation in silico. Different colors represent different states from cluster analyses. GTPases are labelled in each panel.

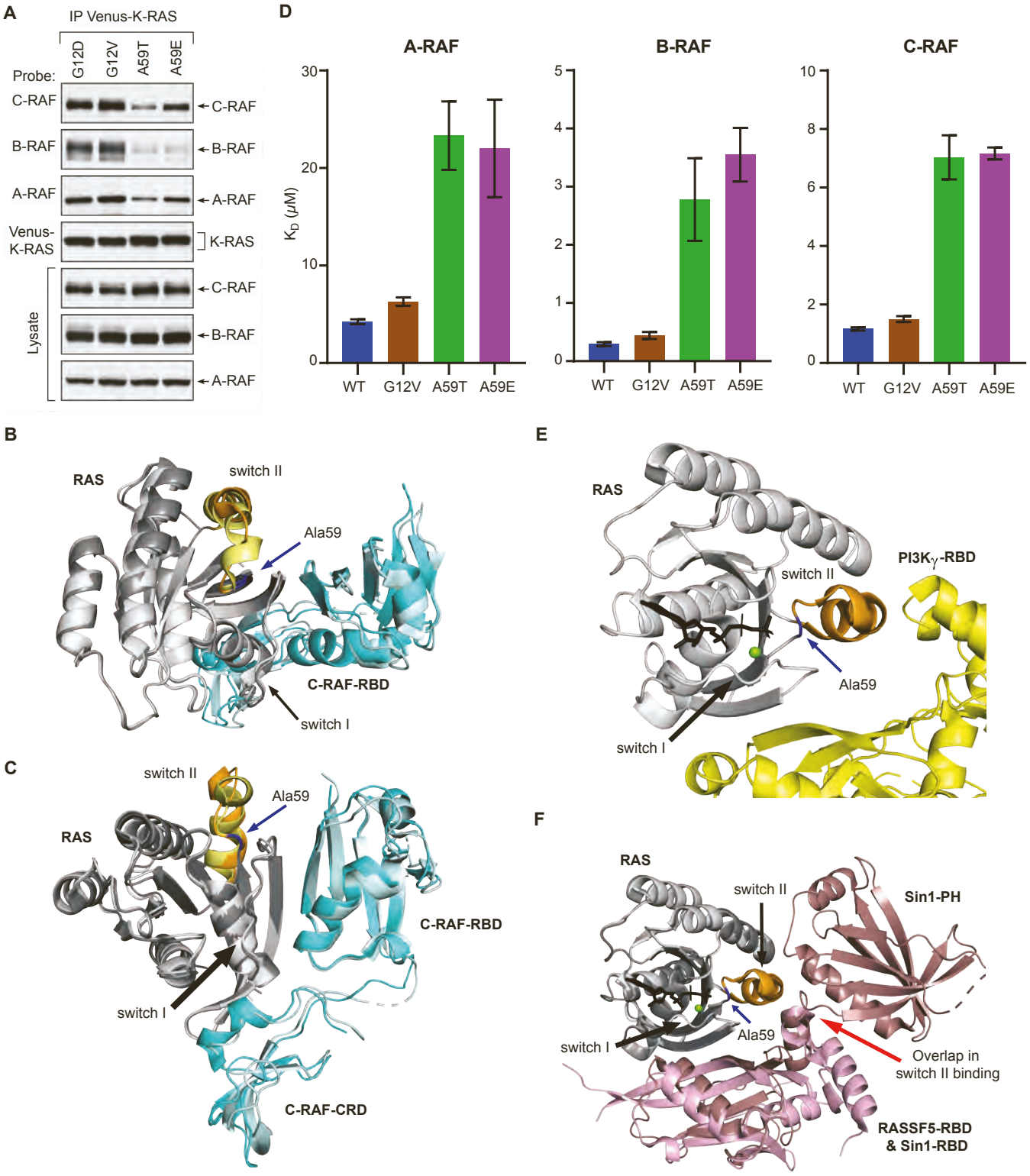

Figure S6. Extended RBD interaction analysis, related to Figure 5.

(A) Western blot of RAF isoforms coimmunoprecipitating with Venus-tagged K-RAS proteins from dividing HeLa cells.

(B-C) Spatial relationship of Ala59 (blue arrow) and switch II (yellow and orange ribbon) of RAS (H-RAS in light grey and K-RAS in dark gray) with the C-RAF-RBD-CRD (light and dark cyan, respectivly) (PDB codes 6XI7 and 7JHP). (C) is a 90˚ rotation of (B).

(D) K_D for GppNHp bound K-RAS (WT, G12V, A59E and A59T mutants) and the RBDs of A-RAF, B-RAF, and C-RAF determined by BLI. Error bars represent standard deviation (n = 2-4).

(E) Spatial relationship of Ala59 (blue arrow) and switch II (orange ribbon) of H-RAS bound to PI3K (yellow) (PDB code 1HE8).

(F) Spatial relationship of Ala59 (blue arrow) and switch II of RAS with the RASSF5-RBD (pink, PDB code 3DDC) and Sin1-RBD-PH (dark pink, PDB code 7LC1). Coloring of RAS proteins as in (C-D).

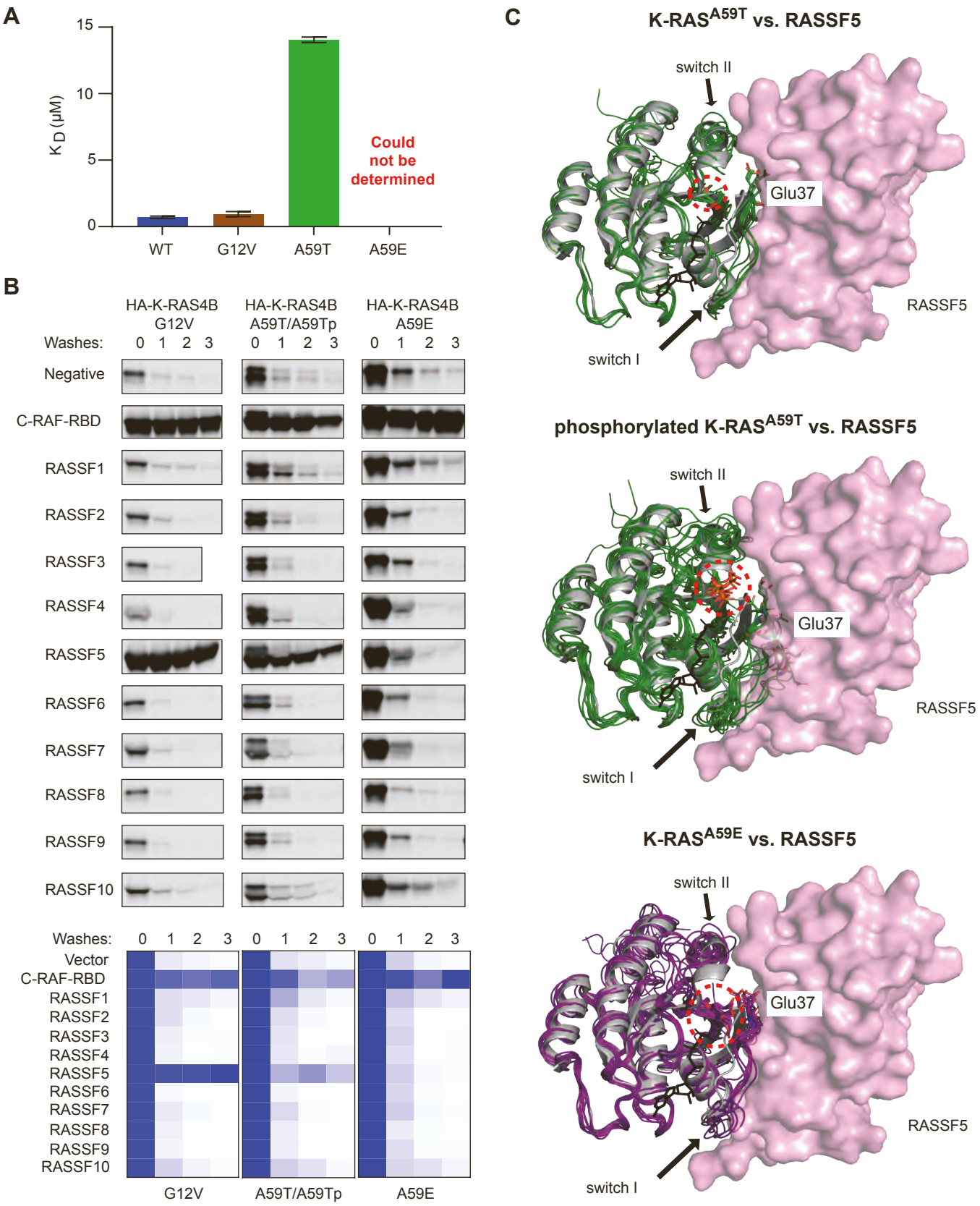

Figure S7. Interaction of phosphorylated K-RAS^{A59T} and K-RAS^{A59E} with RASSF proteins, related to Figure 5.
(A) Affinities of GppNHp bound K-RAS (wild-type, G12V and A59T) for the RA domain of RASSF5 determined by BLI. K-RAS^{A59E} exhibited negligible binding thus a K_D value could not be determined. Error bars represent standard deviation (n = 2-4).
(B) Precipitation experiments testing the affinity of GTP bound HA-KRAS4B and its mutants to different RASSF proteins. Experiments were done as in Figure 5B. Quantification of precipitations (lower panel) were scaled to the '0' wash step (supernatent removal after precipitation, without buffer wash). Note that binding in the K-RAS^{A59T} precipitation set is the combination of both upper and lower bands in the western blot.
(C) For each panel, the wild-type crystal structure of H-RAS is shown as a gray ribbon while simulations are colored strings derived from the same cluster analyses of simulations desribed in Figure 5I. RASSF5-RA domains are shown as colored surfaces. Dotted circles show location of mutation or autophosphorylation.